INL/CON-16-38207
PREPRINT

ELECTRON PROBE MICROANALYSIS OF IRRADIATED AND 1600°C SAFETY-TESTED AGR-1 TRISO FUEL PARTICLES WITH LOW AND HIGH RETAINED ^{110M}AG

2016 ANS Winter Meeting and Nuclear Technology Expo

Karen E. Wright and Isabella J. van Rooyen

November 2016

The INL is a
U.S. Department of Energy
National Laboratory
operated by
Battelle Energy Alliance

ELECTRON PROBE MICROANALYSIS OF IRRADIATED AND 1600°C SAFETY-TESTED AGR-1 TRISO FUEL PARTICLES WITH LOW AND HIGH RETAINED ^{110M}AG

Karen E. Wright[a] and Isabella J. van Rooyen[b]
[a]*Advanced Characterization Department, Idaho National Laboratory,*
PO Box 1625, Idaho Falls, ID 83415-6157
Email: karen.wright@inl.gov
[b]*Fuel Design and Development Department, Idaho National Laboratory,*
PO Box 1625, Idaho Falls, ID 83415-3855

Advanced Gas Reactor (AGR)-1 fuel Compact 4-3-3 achieved 18.63% FIMA and was exposed to a safety test at 1600°C. Two particles, AGR1-433-003 and AGR1-433-007, with measured-to-calculated ^{110m}Ag inventories of <22% and 100%, respectively, were selected for electron microprobe analysis to determine whether the distribution or abundance of fission products differed proximally and distally from the deformed kernel in AGR1-433-003 and how this compared to fission product distribution in AGR1-433-007. On the deformed side of AGR1-433-003, xenon, cesium, iodine, europium, strontium, and tellurium concentrations in the kernel buffer interface near the protruded kernel were up to six times higher than on the opposite, non-deformed side. At the silicon carbide (SiC)-inner pyrolytic carbon (IPyC) interface proximal to the deformed kernel, palladium and silver concentrations were 1.2 and 0.04 wt% respectively. On the SiC-IPyC interface distal from the kernel deformation, those elements measured 0.4 and 0.01 wt%, respectively. Palladium and silver concentrations at the SiC-IPyC interface of AGR1-433-007 were 2.05 and 0.05 wt.%, respectively. Rare earth element concentrations at the SiC-IPyC interface of AGR1-433-007 were ten times higher than at the SiC-IPyC interfaces measured in AGR1-433-003. Palladium permeated the SiC layer of AGR1-433-007 and the SiC layer of the non-deformed side of AGR1-433-003.

I. INTRODUCTION

Several fuel irradiation experiments have been planned for the Advanced Gas Reactor (AGR) Fuel Development and Qualification Program, with the AGR-1 experiment being the first of these experiments.[1] The AGR-1 experiment was performed to test irradiation logistics (such as multi-capsule test train design) and to provide data on fuel performance to aid in its design. Further, AGR-1 provided samples for post-irradiation safety testing where fission product (FP) retention at high temperatures could be measured experimentally.[2]

Tristructural isotropic (TRISO)-coated nuclear fuel kernels are nominally 350 µm in diameter, with a 100-µm buffer layer, a 40-µm inner pyrolytic carbon (IPyC) layer, a 35-µm silicon carbide (SiC) layer, and a 40-µm outer pyrolytic carbon layer that are layered concentrically around the fuel kernel. Fuel tested in the AGR-1 experiment has kernels composed of a mixture of uranium oxide and uranium carbide with a nominal stoichiometry consisting of $UO_{1.37}C_{0.35.}$[3]

FP distribution has been studied in various types of layered nuclear fuel particles for several decades. Schenk and Nabielek[4] used irradiation and subsequent heating tests on UO_2 TRISO particles to determine the fractional release of ^{137}Cs, ^{90}Sr, ^{110m}Ag, and ^{85}Kr. Barrachin et al. studied the distribution of FP in oxide TRISO fuels and used MEPHISTA and MFPR modeling codes to determine the oxygen potential and speciation of the FP in the irradiated fuel.[5] Kleykamp used electron probe microanalysis (EPMA) to determine FP distribution in UO_2 and UC_2 particles irradiated to >50% FIMA.[6] In the oxide particle kernels, Kleykamp found significant metallic inclusions consisting of Mo-Tc-Ru-Rh-Pd and Pd-Te, along with (Sr, Ba)(Zr, U, Re) O_x ceramic inclusions; however, he found nothing analogous in the UC_2 kernels. With both fuel types, Kleykamp noted a 15 µm-thick region surrounding the kernel that he termed the "recoil zone," where higher concentrations of FPs were present. In the recoil zone surrounding the oxide kernel, there were elevated levels of Ba, I, Te, Nd, and Ce, while in the recoil zone surrounding the carbide kernel, Kleykamp observed elevated concentrations of Ce, Nd, Xe, and Cs.

While much of the EPMA study of FP distribution in TRISO particles has been limited to those with UC_2 or UO_2 fuel kernels, relatively little work using EPMA has been performed on TRISO particles with a UCO fuel kernel. Tiegs studied FP distribution in UC_2, UO_2, PuO, ThO_2-PuO, and UCO kernels, with particular attention to corrosion of the SiC layer by Pd.[7,8] However, the UCO particles that Tiegs examined had a C:O ratio of about

4:1, while those in the AGR-1 experiment have a C:O ratio of about 1:4.[3]

Work to-date studying AGR-1 coated particles with UCO kernels has used other analytical or advanced microstructural techniques and has included work performed using scanning electron microscopy montage mapping as a comparative tool in conjunction with energy dispersive spectroscopy, scanning transmission electron microscopy, and high resolution transmission electron microscopic analysis. [9-15] Similar to scanning electron microscopy, the electron interaction volume for EPMA depends on the elemental composition interrogated by the beam, which for UO_2 using a 20-kV accelerating voltage is about 1.4 µm in diameter. While this is much larger than that of scanning transmission electron microscopy or high resolution transmission electron microscopy, the advantage of EPMA is that overlapping analytical peaks so frequently encountered in irradiated fuels can be de-convoluted. This allows for quantitative measurement of FPs on a micrometer scale.

This work describes the distribution of FPs within irradiated, safety-tested AGR-1 particles using EPMA. One of the examined particles has a defect in which the kernel protrudes slightly into the buffer layer. While the observed defect is quite small, it has not been established how large such a defect must be to result in enhanced FP release from the kernel.

We examine whether or not such a defect will result in a loss of FPs from the kernel and whether it will result in an accumulation of FPs proximal to the defect.

II. METHODS

II.A. Irradiation and Safety Testing

TRISO particles in Compact 4-3-3 were constructed using Variant 3 methodology[1] and were subjected to irradiation as described by Demkowicz et al.[2] Following irradiation, the compact was safety tested using the fuel accident condition simulator furnace,[16] which was used to evaluate the release of FPs upon heating. Table I shows the irradiation and safety testing parameters.

Following the safety test, the compact was subjected to a leach-burn-leach test. Details of the test can be found in Demkowicz et al.[2]

Following the leach-burn-leach test, 12 particles were selected for gamma counting. The maximum amount of measured-to-calculated ^{110m}Ag inventory (which serves as an estimate of the fraction retained in the particle) was in particle AGR1-433-007 (1.00), while the minimum amount noted was below the detection limit (i.e., <0.22) for particle AGR1-433-003.

TABLE I. Irradiation and subsequent safety testing parameters of Compact 4-3-3.

Parameter	Value
^{235}U enrichment	19.74
% FIMA average burnup	18.63
Time-average, volume average temperature, °C	1094
Approximate fast fluence (x 10^{25}), n/m^2	4.16
Temperature of fuel accident condition simulator furnace, °C	1600
Time spent at temperature (h)	300

II.B. Sample Preparation and Electron Probe Microanalysis

Each of the two particles was mounted into a separate cylindrical metallography mount holder with Buehler EpoHeat epoxy. The mounts were then polished using standard methods to 1 µm or better and were coated with aluminum to a thickness of approximately 20 nm. Specific details on how the particles were mounted and polished are detailed in Demkowicz et al.[2]

EPMA was accomplished using a Cameca SX 100-R shielded electron microprobe. Most of the standards employed were single-element standards, such as U, Pd, and Ag, while compounds were used for more unstable elements, (such as rare earth phosphates for La and Nd) and other rare earth elements (such as pollucite for Cs and barite for Ba). For some elements, standards are difficult to obtain. In these cases, the standard intensity of the adjacent element X-ray lines was used to interpolate a predicted value. These are referred to as “virtual standards” and were used for Xe and Tc.

II.B.1. Quantitative Spot Analysis

Because the objective of this experiment was to determine differences in FP location and abundance, it was necessary to ensure the number of X-ray counts for each X-ray line in each analysis was maximized as much as practical. To maximize X-ray counts, EPMA was run using an accelerating voltage of 20 kV. For most X-ray lines, a current of 200 nA was used except for Si Kα in the SiC layer, which used a current of 20 nA to avoid excessive dead time with the detector. The count time for each X-ray line varied with its abundance and fluorescence yield; however, in general, analytes were counted 300 to 500 seconds each.

Data were collected and analyzed using Probe for EPMA v. 11.4.2. Peak overlap correction is particularly important for accurate irradiated fuel analysis; extensive peak overlap corrections were employed, particularly for rare earth and noble metal analysis. Phi-rho-z corrections employed were those of Pouchou and Pichoir[17] and the mass absorption coefficients that were used were those of

Farthing and Walker.[18] The step size for data collection varied from 2 μm to 5 μm depending upon the region of the particle being measured.

III. RESULTS

Images showing AGR1-433-003 and AGR1-433-007 are provided in Fig. 1.

Because Kleykamp's[6] "recoil zone" term is used extensively in this work, it is necessary to describe how its location was determined in these samples. Spatially, the recoil zone is the outer perimeter of the kernel, where the kernel interfaces with the buffer layer; in these samples it is about 25 μm thick. Chemically, it is characterized by uranium concentrations that are lower than those in the kernel but are higher than those in the buffer. Likewise, carbon concentrations are higher than those in the kernel, but lower than those in the buffer. These large concentration changes occur linearly over the relatively short (25 μm) thickness of the recoil zone (Fig. 2). Note that in Figure 2, the C concentration in the buffer and IPyC averages about 60 wt. %. This is much lower than expected and is likely due to the combined effects of non-matrix matched standards for carbon and lingering porosity in these layers.

III.A. Analysis of Xe, I and Cs

The Xe, I, and Cs concentrations on the deformed side of the kernel in the recoil zone exceed those measured on the non-deformed side in AGR1-433-003. This is particularly evident when comparing the I and Xe concentrations (Fig. 3). Note that in Figure 3 and all similar figures, the labeled regions (e.g. buffer) are approximate. In addition, there is an epoxy gap present in the IPyC layer near its interface with the buffer layer.

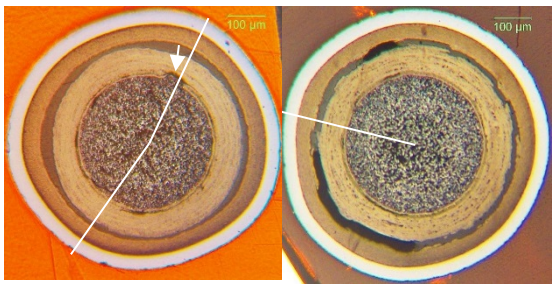

Fig. 1. Optical microscope image of AGR1-433-003 (left) and AGR1-433-007 (right). Paths of measured radial traverses are shown with white lines. The slightly deformed kernel in AGR1-433-003 is shown with the arrow.

When AGR1-433-003 and AGR1-433-007 are compared, it is seen that while the I concentration in the recoil zone of the deformed side of AGR1-433-003 is a factor of approximately two higher than the corresponding area on the non-deformed side and in the recoil zone for AGR1-433-007, the same is not true for Xe. Xe concentration in AGR1-433-007 is slightly higher in the buffer and recoil zone than in the same areas of AGR1-433-003 (Fig. 3). With respect to Cs concentration, there is substantial overlap in all regions measured, with the exception of two points in the recoil zone of AGR1-433-003 and several points in the IPyC-SiC interface, which are somewhat elevated relative to their counterpoints in the other traverses measured.

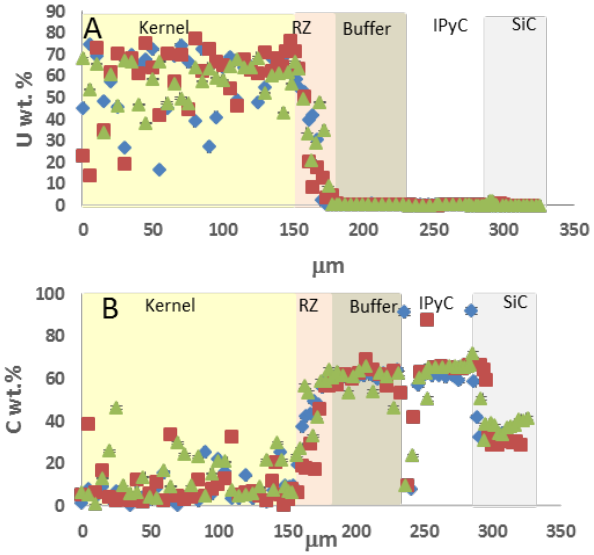

Fig. 2. U concentration (A) and C concentration (B) in AGR1-433-003 and AGR1-433-007. Squares represent the radial traverse on the side with the deformed kernel of AGR1-433-003; diamonds represent the radial traverse on the intact side. Triangles represent AGR1-433-007. Where no error bars are visible, the error is smaller than the symbol.

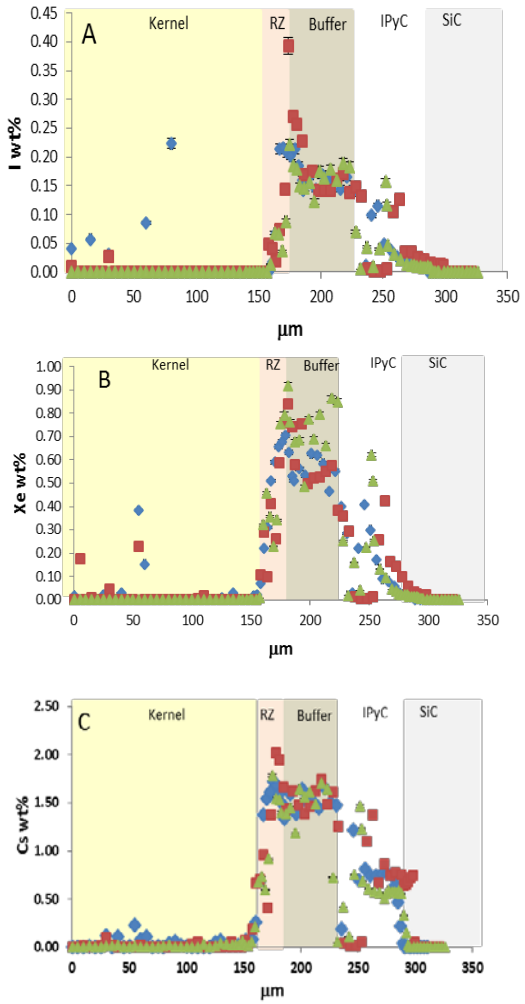

Fig. 3. I concentration (A), Xe concentration (B), and Cs concentration (C) in AGR1-433-003 and AGR1-433-007. Squares represent the radial traverse on the side with the deformed kernel of AGR1-433-003 and diamonds represent the radial traverse on the intact side. Triangles represent AGR1-433-007. If no error bars are visible, then the error is smaller than the symbol.

III.B. Analysis of Europium, Tellurium, and Strontium

Europium, Te, and Sr FP concentrations are up to six times higher in the recoil zone of the deformed side of the AGR1-433-003 kernel than on the non-deformed side of the kernel (Fig. 4). They also exceed those in AGR1-433-007, but by a much smaller margin. Unlike other FP, significant elevations of Eu, Te, and Sr are limited to the recoil zone.

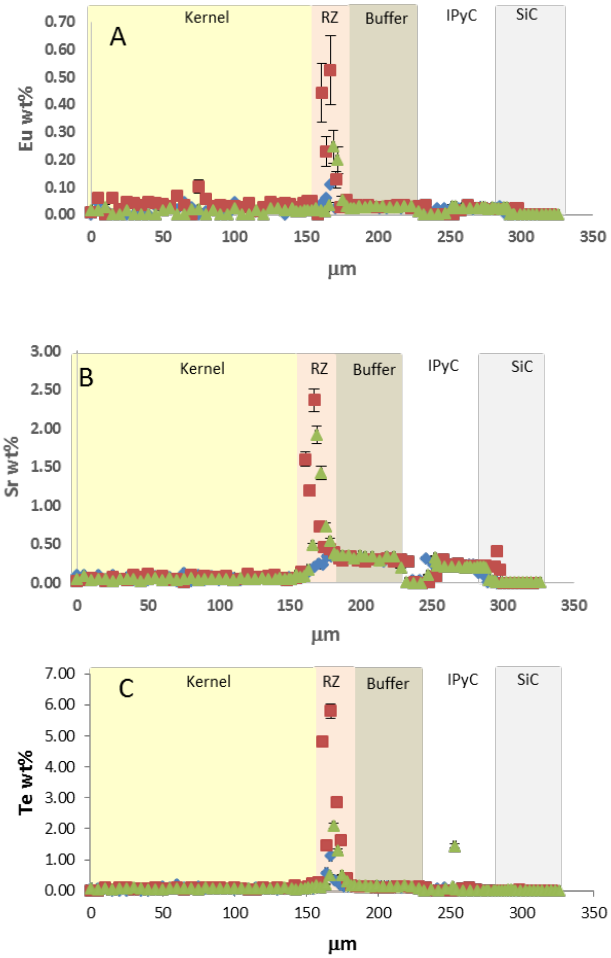

Fig. 4. Eu concentration (A), Sr concentration (B), and Te concentration (C) in AGR1-433-003 and AGR1-433-007. Squares represent the radial traverse on the side with the deformed kernel of AGR1-433-003 and diamonds represent the radial traverse on the intact side. Triangles represent AGR1-433-007. If no error bars are visible, then the error is smaller than the symbol.

III.C Analysis of Zirconium, Molybdenum, Ruthenium, and Technetium

Zirconium and Mo behave similarly to Ru in that, for all examined areas, the highest concentrations are generally found in the kernel and there are no significant differences between either side of AGR1-433-003 and AGR1-433-007. In the recoil zone, concentrations for all three of these elements rapidly fall to <0.1 wt%, but remain detectable (Fig. 5). Detection limits vary with each element and matrix in which the element occurs. They are calculated for each analysis but in general can be approximated by counts that exceed three standard deviations above the average background.

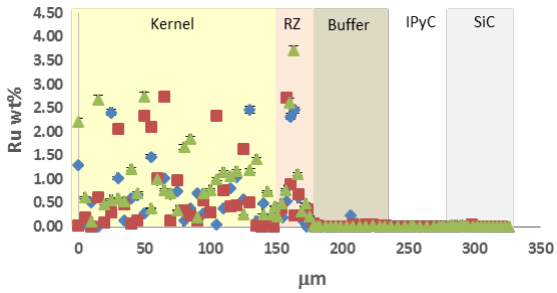

Fig. 5. Ru concentration in AGR1-433-003 and AGR1-433-007. Squares represent the radial traverse on the side with the deformed kernel of AGR1-433-003; diamonds represent the radial traverse on the intact side. Triangles represent AGR1-433-007. Where no error bars are visible, the error is smaller than the symbol.

In contrast, there are several locations within the kernel where the concentration of Tc on the non-deformed side of AGR1-433-003 is two to three times higher than that on the deformed side. Tc is similarly elevated in the kernel of AGR1-433-007 (Fig. 6), suggesting the possibility that Tc precipitates are present in the non-deformed side of AGR1-433-003 and AGR1-433-007, but are not present or are much smaller on the deformed side of AGR1-433-003.

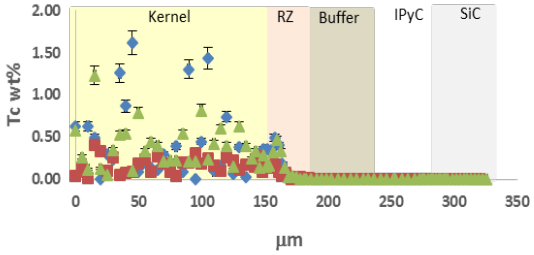

Fig. 6. Tc concentration in AGR1-433-003 and AGR1-433-007. Squares represent the radial traverse on the side with the deformed kernel of AGR1-433-003; diamonds represent the radial traverse on the intact side. Triangles represent AGR1-433-007. Where no error bars are visible, the error is smaller than the symbol.

III.D. Analysis of Cerium, Lanthanum, Samarium, Praseodymium, and Neodymium

FP distributions appear similar in both AGR1-433-003 and AGR1-433-007 for Ce, La, Sm and Pr. For all four of these elements, the highest concentration is in the kernel, but it rapidly diminishes in the recoil zone to low (<0.05 wt%), but generally detectable, concentrations (Fig. 7 (A through D)). However, the behavior of Nd is different. The concentration of Nd in the AGR1-433-003 kernel (non-deformed side) is up to 100% higher than the analogous region of the deformed side of AGR1-433-003 or the kernel of AGR1-433-007 (Fig. 7E).

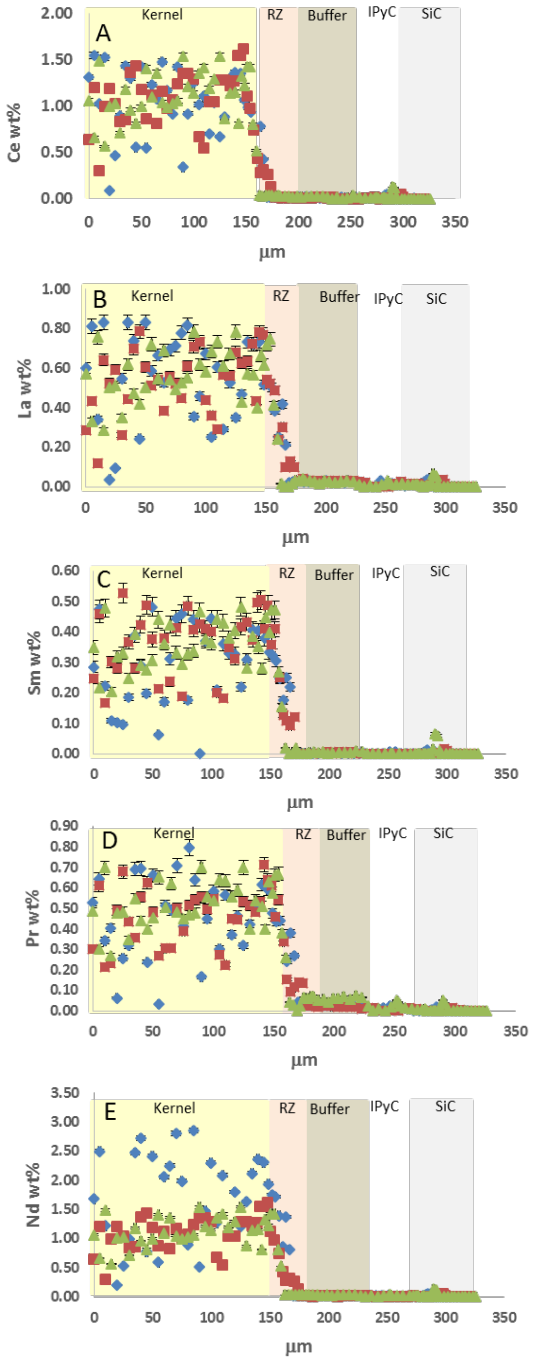

Fig. 7. Ce concentration (A), La concentration (B), Sm concentration (C), Pr concentration (D), and Nd concentration (E) in AGR1-433-003 and AGR1-433-007. Squares represent the radial traverse on the side with the deformed kernel of AGR1-433-003; diamonds represent the radial traverse on the intact side. Triangles represent AGR1-433-007. Where no error bars are visible, the error is smaller than the symbol.

III.E. Analysis of Palladium, Cadmium, Tin, and Silver

With regard to Pd and Cd, there is very little difference in the observed accumulations of these elements in any of the examined kernel locations. While Cd is not detected beyond the buffer zone, Pd accumulates at the SiC-IPyC interface as small precipitates (Fig. 8 A and B). Tin is present in small amounts (<0.05 wt.%) for most examined kernel areas, with only two points exceeding that amount; it also accumulates along the SiC-IPyC interface (Fig. 8C) in both AGR1-433-003 and AGR1-433-007 and is marginally greater in concentration in AGR1-433-007. Tin is also elevated at the kernel-recoil zone interface. With regard to Ag, AGR1-433-003 shows elevated concentrations (up to about 1 wt.%) on both measured sides of the AGR1-433-003 kernel, while Ag was not detected in the AGR1-433-007 kernel (Fig. 8D). In addition, in the recoil zone on the deformed side of AGR1-433-003, Ag was elevated as high as 0.45 wt%, but was measured at 0.045 wt% on the non-deformed side of AGR1-433-003 and not detected in AGR1-433-007.

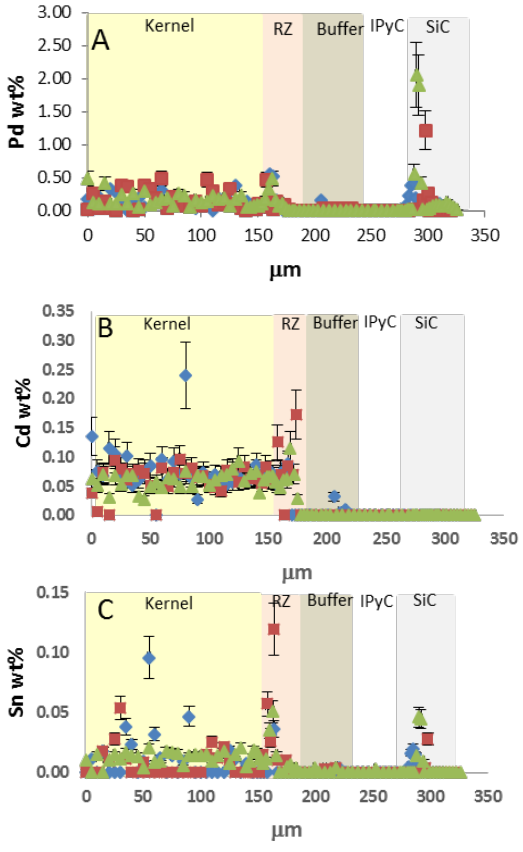

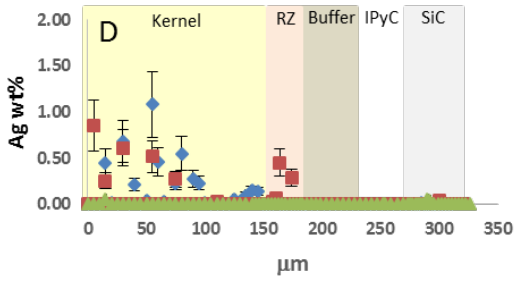

Fig. 8. Pd concentration (A), Cd concentration (B), Sn concentration (C), and Ag concentration (D) in AGR1-433-003 and AGR1-433-007. Squares represent the radial traverse on the side with the deformed kernel of AGR1-433-003; diamonds represent the radial traverse on the intact side. Triangles represent AGR1-433-007. Where no error bars are visible, the error is smaller than the symbol.

At the SiC-IPyC interface, Ag concentrations along measured traverses were highest in AGR1-433-007 at 0.05 wt%, while the deformed side of AGR1-433-003 measured 0.04 wt% and the non-deformed side of AGR1-433-003 measured 0.01 wt%.

The differences in silver location and abundance will be addressed in more detail in section IVB.

IV. DISCUSSION

IV.A. Effect of Kernel Protrusion on Fission Product Distribution and Concentration from Particle AGR1-433-003 (Deformed Side versus Non-Deformed Side)

Upon observing the incipiently deforming kernel on one side of AGR1-433-003, we sought to determine whether FP release from the kernel would be more extensive on the deformed side compared to the non-deformed side. Because elements such as Xe and Cs are released significantly by the kernel into the buffer[5], it is plausible that kernel deformation may enhance that effect.

With regard to I, Xe, Cs, Te, Sr, Sn, and Eu, the concentration of these elements in the recoil zone proximal to the kernel defect is notably higher than in the recoil zone distal from the defect. In addition, Nd and Tc concentrations in the kernel on the non-deformed side are elevated relative to those on the deformed side. Palladium, which is of interest due to its corrosive effect on the SiC layer, is higher in concentration at the SiC-IPyC boundary on the deformed side of the kernel compared to the SiC-IPyC boundary on the non-deformed side of the kernel.

However, when the elevated FP concentrations in AGR1-433-003 are compared to the nominal concentrations observed in AGR1-433-007, it can be seen that the some of the FP concentrations in AGR1-433-007 exceed the highest concentrations seen in AGR1-433-003. For example Xe concentrations in AGR1-433-007 are

higher in the recoil zone and buffer than the highest concentrations observed in those regions in AGR1-433-003 (Fig. 3). At the SiC-IPyC interface, Pd concentration in AGR1-433-007 is twice the concentration observed on the SiC-IPyC interface on the deformed side of AGR1-433-003 (Fig. 8A). With regard to the Sr and Eu concentrations in the recoil zone, those in AGR1-433-007 exceed those observed on the non-deformed side of AGR1-433-003, but are not as high as the highest concentrations on the deformed side (Fig. 4).

Table II shows the depth of FP penetration into the SiC layer for both radial traverses of AGR1-433-003 and one radial traverse of AGR1-433-007. All measured elements, except Ag, Pr, and Te penetrate deeper into the SiC layer of the non-deformed side of AGR1-433-003 compared to the deformed side, while I and Tc become undetectable at the SiC-IPyC boundary of both the deformed and non-deformed side. While penetration depth for most FPs is similar in AGR1-433-007 to the non-deformed side of AGR1-433-003, for the elements La, Ce, Nd, Pr, Sm, Mo, U, and Pd, the highest concentration observed at the SiC-IPyC interface is at least double in AGR1-433-007 compared to same interface of either side of AGR1-433-003 (Fig. 9, Table II).

TABLE II. Penetration of analyzed elements into the SiC layer. “Interface” indicates the element was found at the IPyC-SiC boundary. “ND” indicates the element was not detected. “Throughout” indicates the element was found intermittently or continuously throughout the SiC layer. The concentration value indicates the highest concentration found in the SiC-IPyC interfacial region. Concentration values in red are the highest noted for the three interfacial regions measured.

Element	AGR1-433-003 Deformed Side SiC Penetration (µm)	Highest Concentration in Interface (wt.%)	AGR1-433-003 Non-Deformed Side SiC Penetration (µm)	Highest Concentration in Interface (wt.%)	AGR1-433-007 SiC Penetration (µm)	Highest Concentration in Interface (wt.%)
I	Interface	0.013	Interface	0.011	Interface	0.007
Xe	Interface	0.020	6	0.013	6	0.014
Cs	6	0.074	20	0.64	20	0.56
Ba	2	0.61	18	0.58	6	0.63
Sr	Interface	0.41	10	0.20	Throughout	0.20
Eu	Interface	0.024	14	0.032	Interface	0.028
La	2	0.037	4	0.033	4	0.067
Ce	2	0.049	Throughout	0.050	4	0.125
Nd	2	0.064	4	0.051	4	0.15
Pr	6	0.015	4	0.019	4	0.051
Sm	2	0.016	4	0.011	4	0.065
Ru	Interface	0.042	4	0.016	4	0.034
Mo	Interface	0.005	6	0.005	4	0.056
Zr	Interface	0.022	6	0.023	4	0.013
Tc	Interface	0.008	Interface	0.004	4	0.008
U	2	1.14	Throughout	0.51	4	1.98
Pd	6	1.21	Throughout	0.42	Throughout	2.05
Cd	ND		ND		ND	
Ag	2	0.037	Interface	0.016	2	0.052
Sn	Interface	0.028	4	0.020	4	0.040
Te	Interface	0.030	ND		4	0.032

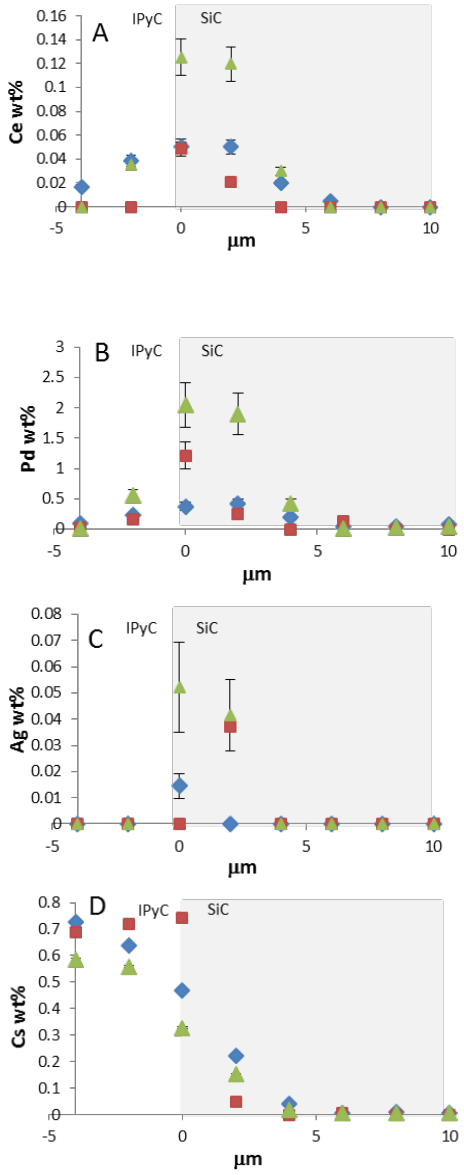

Fig. 9 (A through D): Ce, Pd, Ag, and Cs wt%, respectively, across the IPyC-SiC interface. Squares represent the radial traverse on the side with the deformed kernel of AGR1-433-003; diamonds represent the radial traverse on the intact side. Triangles represent AGR1-433-007. Where no error bars are visible, the error is smaller than the symbol.

IV.B. Location of Silver

The location of silver and its release from TRISO particles is of particular interest to researchers because of the risk ^{110m}Ag release poses to workers when it deposits on cooler metallic parts of the helium pressure boundary [19]. In the studied particles, AGR-1-433-003 retained less than 22% of its predicted ^{110m}Ag inventory while particle AGR1-433-007 retained 100%. Because of the substantial difference in silver retention between the two particles and the risk posed by silver release, it is worth examining the differences in silver distribution between the two particles, bearing in mind that a detailed discussion of silver speciation and transport is outside the scope of this paper.

As Fig. 8D shows, small, sporadic elevated concentrations of Ag in AGR1-433-003 are present in the kernel of both radial traverses; yet in AGR1-433-007, no Ag was detected along the measured traverse, except at the IPyC-SiC interface. However, inspection of the IPyC-SiC interface in AGR1-433-007 shows an arc of approximately 110 degrees, which contains abundant Ag-Pd-U precipitates (Fig. 10), many of which penetrate the SiC layer. The analogous interface in AGR1-433-003 contains very few precipitates and the precipitates that are present are much smaller (<1 µm) compared to those seen in AGR1-433-007.

This observation contrasts with SEM analysis of particles AGR1-433-001 and AGR1-433-004. Precipitate clusters in these particles were reported to occur in great abundance along the entire circumference of the SiC-IPyC interface [11, 20-21].

It is not possible to get a very accurate analysis of the precipitates using EPMA. They are typically smaller than the electron beam interaction volume, which means that the beam may measure more than one particle or will include a large amount of matrix (e.g. C or SiC) in the analysis. However, it is possible to make some general comparisons between particles. Firstly, along the 110-degree precipitate-rich arc along the SiC-IPyC interface in AGR1-433-007, a total of forty-two precipitates were identified and analyzed. The average Pd, Ag and U concentrations were 3.1, 0.14, and 3.1 wt%, respectively. The highest concentration of these elements measured at the SiC-IPyC interface on the other side of AGR1-433-007 was 0.4, 0.014, and 0.5 wt%, respectively. This means that the precipitates on the precipitate-rich side were larger, had a greater concentration of those elements, or both, compared to the other side.

This suggests the presence of a lateral temperature gradient across the particle (Pd precipitates on the cold side of the particle).[22] While the mechanism for Pd-Ag-U precipitation on the cold side of the particle is unclear, both Tiegs[7] and Minato et al.[22] describe this effect. Tiegs[7] specifically describes the transport of Pd and rare earth elements

down the temperature gradient. Grubmeier et. al [23] noted diffusion of heavy metals toward the cool side of the particle, to include rare earth and platinum group elements; however, they noted that rare earth and platinum group elements were not necessarily co-located.

The phenomena of temperature gradients in TRISO particles and its relationship to ^{110m}Ag migration and release is complex. Most of the AGR-1 compacts exhibit a large range of ^{110m}Ag release [24] driven primarily by the temperatures experienced by the fuels during irradiation. For example, approximately half of the particles in AGR-1 compact 4-3-3 experienced temperatures of 1300ºC or more for at least 100 days. In contrast, approximately half the particles rarely exceed temperatures of 1000ºC [25]. When comparing particles AGR1-433-003 and AGR1-433-007, it is unclear why the particle that retained <22% of its ^{110m}Ag exhibited elevated concentrations of silver in the kernel whereas the particle that retained 100% of its ^{110m}Ag had no detected silver in the kernel. Instead, this particle's silver inventory appeared to be entirely concentrated along the SiC-IPyC interface. However, because silver diffusion will be driven by temperature, it is possible that differing temperature gradients and regimes experienced by different particles within the same compact may in part explain the contrasts in silver distribution between the two particles.

Because of the possible influence of a temperature gradient on the distribution and precipitation of fission products, it is not possible to determine whether the differences in fission product distribution found on the deformed versus non-deformed side of AGR1-433-003 are due to kernel protrusion, or a temperature gradient (or some other unidentified factor). More investigation is required to clarify how temperature gradients impact migration and deposition of fission products, particularly silver.

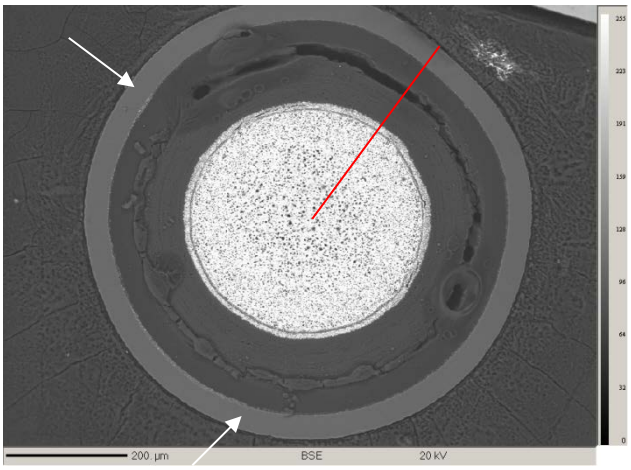

Fig. 10. Backscattered electron images of AGR1-433-007 showing the 110-degree arc of precipitates (between the arrows) along the SiC-IPyC interface. The line indicates the path of the measured analytical traverse.

IV.C. Comparison with Other Analyzed TRISO Particles

Putting these results in context of the results from FP distributions in other EPMA-analyzed TRISO particles is difficult for several reasons. First, many of the previous studies were performed decades ago (e.g., Kleykamp[6] and Tiegs[7]) on particles that were not the same fuel composition as those studied here, nor were the experimental conditions similar. In addition, many other researchers use EPMA as a qualitative tool for determining the presence or non-presence of elements and relative concentrations (e.g., Barrachin et al.[5]), whereas analyses in this effort are quantitative.

However, some similarities can be found. For example, both Barrachin et al.[5] and Kleykamp[6] observe elevated concentration of Xe and Cs in the buffer, relative to what remains in the kernel. Kleykamp[6] also report elevated I. These observations are similar to what we see in our samples (Fig. 3). The mechanism for the loss of these elements from the kernel is explained in detail by Barrachin et al.[5]. In brief, they suggest that a large portion of Xe remains in atomic form in the fuel matrix and moves by diffusion toward grain boundaries. Once it reaches the grain boundaries, it can travel via interconnected pores formed by high temperatures. The mechanism for Cs movement is similar, except that they postulate that Cs can travel as an oxide or iodide.

In his analysis of irradiated TRISO with a UO_2 kernel, Kleykamp[6] made the following observations, which are very similar to our own:

1. While Ce, Nd, Pr, and Pd are close to the detection limit within the buffer layer and are

somewhat elevated in the IPyC, their concentration increases by a factor of up to 10 at the IPyC-SiC interface. This can be seen in Figure 9 (A-B).

2. There are large increases in the concentration of Cs, I, and Xe in the recoil zone surrounding the buffer. In this 15 to 20 µm-thick zone, the concentration of these analytes increases rapidly up to a factor of 10 above what they were in the kernel, then decreases rapidly in the buffer.
3. Elements such as Pd are concentrated along the IPyC-SiC interface, but are not symmetrically distributed. Kleykamp[6] referred to this phenomenon as the result of an "azimuthal temperature gradient," where he noted the presence of Pd and Te precipitates on the cold side of the particle. Minato described similar precipitates occurring on the cold side of the particle.[22]

Tiegs[7] elaborated on the effect of temperature on the distribution of FPs when he observed that at temperatures lower than 1400˚C, Pd penetrates the SiC faster than rare earths, whereas at temperatures above 1400˚C, the converse is true. For our samples, which were irradiated at a volume-average, time-averaged temperature of about 1100˚C and safety tested at 1600˚C, it is possible that the resulting distribution of FPs is influenced by both irradiation and safety testing. For AGR1-433-003, rare earth penetration into the SiC layer proximal to the deformed kernel is about 2 µm, except for Pr, which was detected at 6 µm. Pd penetration was also 6 µm on that side. On the non-deformed side, rare earth penetration was 4 µm, except for Ce, which was detected sporadically throughout the SiC layer. Unlike the deformed side in which Pd penetration did not exceed 6 µm, Pd on the non-deformed side was detected continuously throughout the SiC layer. For AGR1-433-007, no rare earth elements were detected past 4 µm into the SiC layer, while Pd was detected continuously throughout the SiC layer. Because Pd penetration into the SiC was generally deeper and more continuous than that of the rare earths, it suggests that FP distribution observed at the SiC-IPyC interface is largely controlled by irradiation, not the subsequent safety testing.

V. CONCLUSIONS

- Concentrations of I, Cs, and Xe in the recoil zone on the deformed side of AGR1-433-003 were up to two times higher than in the recoil zone on the non-deformed side of the kernel. Concentration of Xe in the recoil zone of AGR1-433-007 was 10% higher than that in the recoil zone of the deformed side of AGR1-433-003.
- Eu, Sr, and Te concentrations in the recoil zone are up to six times higher on the deformed side of AGR1-433-003 compared to the non-deformed side. For the recoil zone of AGR1-433-007, these elements are up to four times higher than those in the recoil zone of the non-deformed side of AGR1-433-003.
- At the SiC-IPyC interface of AGR1-433-007, rare earth element, U, and Pd concentrations are up to two times higher than at either interface side of AGR1-433-003; Mo is ten times higher. At the SiC-IPyC interface of AGR1-433-003, Sr and Ru concentrations are approximately two times higher on the deformed side than on the non-deformed side. I, Xe, and Cs are up to 50% higher at the SiC-IPyC interface on the deformed side compared to the non-deformed side or the SiC-IPyC interface of AGR1-433-007.
- Volatile FPs such as Cs, I, and Xe are not retained in the kernel, but rather they accumulate significantly in the buffer.
- FP accumulation outside the deformed region of the kernel is greater than outside the non-deformed region of the same kernel; however, a kernel showing no similar aberrations shows larger accumulation of FPs along the SiC-IPyC interface, suggesting that FP migration and precipitation may be more strongly influenced by factors other than kernel integrity.
- The particle that retained all its predicted ^{110m}Ag inventory had extensive Pd-Ag deposits along a 110-degree arc within the SiC-IPyC interface, while the particle that had <22% of its predicted ^{110m}Ag inventory had a paucity of such deposits. Asymmetry of Pd-Ag deposits is suggestive of a lateral temperature gradient within particle AGR1-433-007, wherein the precipitates are more common on the cold side of the particle.

ACKNOWLEDGEMENTS

This work was sponsored by the U.S. Department of Energy's Office of Nuclear Energy, under U.S. Department of Energy Idaho Operations Office Contract DE-AC07-05ID14517, as part of the Advanced Reactor Technology Program. We thank Scott Ploger of Idaho National Laboratory (retired) for his optical microscope images and Dr. Paul Demkowicz of Idaho National Laboratory for providing data concerning experiment set up and execution.

REFERENCES

1. J. MAKI, *AGR-1 Irradiation Experiment Test Plan*, INL/EXT-05-00593, Revision 3.
2. P. A. DEMKOWICZ, S. A. PLOGER, and P. L. WINSTON, *AGR-1 Compact 4-3-3 Safety Testing and Post-Test Examination Results*, INL/EXT-16-38287.
3. J. D. HUNN, *Results from ORNL Characterization of Nominal 350 µm NUCO Kernels from the BWXT 69300 Composite*, ORNL/CF-04/07.
4. W. SCHENK and H. NABIELEK, "High-Temperature Reactor Fuel Fission Product Release and Distribution at 1600 to 1800°C," *Nucl Technol*, 96, 323-336 (1991).
5. M. BARRACHIN, R. DUBOURG, S. DE GROOT, M. P. KISSANE, and K. BAKKER, "Fission-product behavior in irradiated TRISO-coated particles: Results of the HFR-EU1bis experiment and their interpretation," *J Nucl Mater*, 415, 104-116 (2011).
6. H. KLEYKAMP, *Mikrosondenuntersuchungen zum Verhalten der Spalprodukte in hoch abgebrannten HTR-brennstoffen, Kernforschungszentrum Karlsruhe*, Report KfK 2213.
7. T. N. TIEGS, *Fission Product Pd-SiC Interaction in Irradiated Coated Particle Fuels*, ORNL/TM-7203.
8. T. N. TIEGS, "Fission Product Pd-SiC Interaction in Irradiated Coated-Particle Fuels," *Nucl Technol*, 57, 389-398 (1982).
9. I. J. VAN ROOYEN, Y. Q. WU, and T. M. LILLO, "Identification of Silver and Palladium in Irradiated TRISO Coated Particles of the AGR1 Experiment," *J Nucl Mater*, 446, 178-186 (2014).
10. I. J. VAN ROOYEN, D. JANNEY, B. MILLER, P. DEMKOWICZ, and J. RIESTERER, "Electron microscopic evaluation and fission product identification in irradiated TRISO coated particles from the AGR-1 experiment: A preliminary review," *Nucl Eng Des*, 271, 114-122 (2014).
11. I. J. VAN ROOYEN, C. HILL, and T. TROWBRIDGE, "Fission product distribution patterns as a comparative characterization tool for TRISO fuel performance," *TMS2015*, 144th Annual meeting, Walt Disney World Orlando, Florida, March 15 through 19, 2015.
12. T. LILLO and I. J. VAN ROOYEN, "Distribution of Pd, U and Ag in the SiC Layer of Irradiated TRISO Fuel," *J Nucl Mater*, 97-106 (2015).
13. B. LENG, I. VAN ROOYEN, Y. WU, I. SZLUFARSKA, and K. SRIDHARAN, "STEM/EDS Analysis of Fission Products in Irradiated TRISO Coated Particles of the AGR-1 Experiment," *J Nucl Mater*, 475, 62-70 (2016).
14. H. WEN, I. J. VAN ROOYEN, C. HILL, T. TROWBRIDGE, and B. CORYELL, "Fission product distribution in TRISO coated particles neutron irradiated to 3.22 X 10^{25} n/m^2 fast fluence at 1092°C," *ASME Power and Energy 2015*, San Diego, California, June 28 through July 2, 2015.
15. H. WEN, I. J. VAN ROOYEN, J. D. HUNN, T. J. GERCZAK, C. A. BALDWIN, and F. C. MONTGOMERY, "Advanced electron microscopy study of fission product distribution in the failed SiC layer of a neutron irradiated TRISO coated particle," *Microscopy and Microanalysis 2015 (M&M2015)*, Portland, Oregon, August 2 through 7, 2015.
16. P. A. DEMKOWICZ, E.L. REBER, D. M. SCATES, L. SCOTT, "First High Temperature Safety Tests of AGR 1 TRISO fuel with the Fuel Accident Condition Simulator (FACS) Furnace," *J Nucl Mater*, 464, 320-330 (2015).
17. J. L. POUCHOU AND F. PICHOIR, 1991, "Quantitative Analysis of Homogeneous or Stratified Microvolumes Applying the Model," "PAP" in K.F.J. Heinrich and D. E. Newbury (eds.), *Electron Probe Quantification*, New York, Plenum Press, 31-76.
18. I. R. FARTHING and C. T. WALKER, "Heinrich's Mass Absorption Coefficients for the K, L, and M Lines," The European Commission, Institute for Transuranium Elements, Karlsruhe, Report K0290140, 1990.
19. I.J. VAN ROOYEN, T.M. LILLO, Y.Q. WU, "Identification of Silver and Palladium in Irradiated TRISO Coated Particles of the AGR-1 Experiment," *J Nucl Mater*, 446, 178-186 (2014).
20. P.A. DEMKOWICZ, J.D. HUNN, R.N. MORRIS, I. VAN ROOYEN, T. GERCZAK, J.M. HARP, S.A., *AGR-1 Post Irradiation, Examination Final Report*, INL/EXT-15-36407
21. I.J. VAN ROOYEN, C. HILL, H. WEN, T. TROWBRIDGE, 2015, *Scanning Electron Microscopic Examination of Irradiated TRISO Coated Particles of Compacts 4-1-1, 5-3-1, 1-3-1 and Safety Tested Compact 4-3-3 of AGR-1 Experiment*, INL external report in preparation, INL/EXT-15-36278.
22. K. MINATO, T. OGAWA, S. KASHIMURA, K. FUKUDA, M. SHIMIZU, Y. TAYAMA, and I. TAKAHASHI, "Fission Product Palladium-

Silicon Carbide Interaction in HTGR Fuel Particles," *J Nucl Mater*, 192, 184-196 (1990).
23. H. GRUBMEIER, A. NAOUMIDIS, B.A. THIELE, "Silicon Carbide Corrosion in High-Temperature Gas-Cooled Reactor Fuel Particles," *Nucl Tech*, 35, 413-427 (1977)
24. P.A. DEMKOWICZ, J.D. HUNN, S.A. PLOGER, R.N. MORRIS, C.A. BALDWIN, J.M. HARP, P.L. WINSTON, T.J. GERCZAK, I.J VAN ROOYEN, F.C. MONTGOMERY, C.M. SILVA, "Irradiation Performance of AGR-1 High Temperature Reactor Fuel," *Nucl Eng Des*, 306, 2-13 (2016)
25. G. HAWKES, "AGR-1 Daily As-Run Thermal Analysis," In ECAR-968 Rev. 3, Idaho National Laboratory, Idaho Falls, Idaho USA